Progress in Biomaterials (2021) 10:131–150
https://doi.org/10.1007/s40204-021-00158-3

ORIGINAL RESEARCH

Cell encapsulated and microenvironment modulating microbeads containing alginate hydrogel system for bone tissue engineering

Induvahi Veernala[1] · Purandhi Roopmani[1] · Ruby Singh[1] · Uzma Hasan[2] · Jyotsnendu Giri[1]

Received: 9 December 2020 / Accepted: 22 May 2021 / Published online: 5 July 2021

Abstract

Functional tissue regeneration using synthetic biomaterials requires proliferation and heterotypic differentiation of stem/progenitor cells within a specialized heterogeneous (biophysical–biochemical) microenvironment. The current techniques have limitations to develop synthetic hydrogels, mimicking native extracellular matrix porosity along with heterogeneous microenvironmental cues of matrix mechanics, degradability, microstructure and cell–cell interactions. Here, we have developed a microenvironment modulating system to fabricate in situ porous hydrogel matrix with two or more distinct tailored microenvironmental niches within microbeads and the hydrogel matrix for multicellular tissue regeneration. Electrosprayed pectin-gelatin blended microbeads and crosslinked alginate hydrogel system help to tailor microenvironmental niches of encapsulated cells where two different cells are surrounded by a specific microenvironment. The effect of different microenvironmental parameters associated with the microbead/hydrogel matrix was evaluated using human umbilical-cord mesenchymal stem cells (hUCMSCs). The osteogenic differentiation of hUCMSCs in the hydrogel matrix was evaluated for bone tissue regeneration. This will be the first report on microenvironment modulating microbead-hydrogel system to encapsulate two/more types of cells in a hydrogel, where each cell is surrounded with distinct niches for heterogeneous tissue regeneration.

✉ Jyotsnendu Giri
enarm@bme.iith.ac.in

[1] Department of Biomedical Engineering, Indian Institute of Technology, Hyderabad, Kandi, Telangana, India

[2] Department of Biotechnology, Indian Institute of Technology, Hyderabad, Kandi, Telangana, India

Graphic abstract

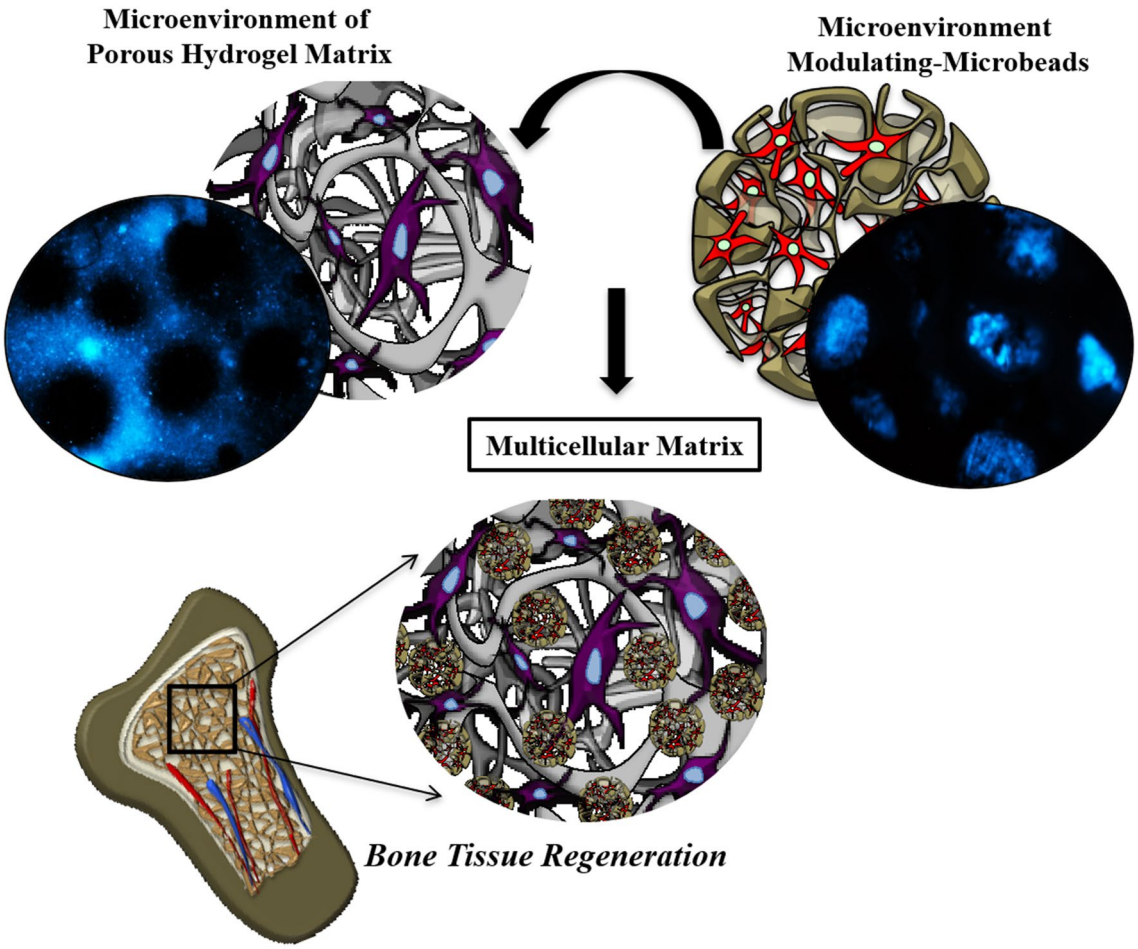

Keywords Microenvironment modulating microbead · Microenvironment modulating hydrogel · Stem cells · Tissue engineering · Electrospraying

Introduction

Stem cells hold great promise for numerous applications such as regenerative medicine, personalized disease model and drug screening (Lian et al. 2010; Mahla 2016). Each of these applications requires stem cells to expand in their naïve state or differentiate into specific lineages, which remains challenging (Baksh et al. 2004; Mahla 2016; Nichols and Smith 2009). The native stem cell niche, comprising of the specialized biophysical and biochemical microenvironment, is crucial to direct the stem cell's fate (Augello et al. 2010; Kolf et al. 2007). Inspired by the native stem cell niche, efforts have been made to develop a broad range of materials and related techniques for developing engineered hydrogel platforms to regulate stem cell fate by controlling microenvironmental parameters such as matrix mechanics, degradability, cell-adhesive ligand presentation, microstructure, porosity and cell–cell interactions (Madl and Heilshorn 2018; Rosales and Anseth 2016).

Stem cells encapsulated alginate hydrogel have been extensively used for tissue engineering applications due to their easy preparation and tenable biophysical properties such as degradation, biocompatibility, non-antigenicity and matrix mechanics (Jeon et al. 2009; Sun and Tan 2013; Yan et al. 2016). Mesenchymal stem cells (MSC) in the alginate 3D hydrogel matrix differentiates into different lineages such as osteogenic, myogenic and neurogenic depending upon the elastic moduli (Pek et al. 2010; Yao et al. 2016) and time-dependent mechanical properties(Sánchez et al. 2020) of the substrate. Similarly, hydrogel matrix degradation

plays an important role in the mechanosensitive differentiation of stem cells (Guvendiren and Burdick 2013). MSCs differentiate into adipogenic and osteogenic lineages when encapsulated into non-degrading hyaluronic acid hydrogels and degradable hydrogels, respectively, regardless of the matrix stiffness (Duarte Campos et al. 2015; Zhao et al. 2014). Khetan et al. demonstrated that matrix degradation is required for tension generation of encapsulated MSCs for osteogenic differentiation (Khetan et al. 2013).

Moreover, regeneration of functional tissue requires a co-delivery of stem cells along with two or more types of cells (Grainger et al. 2013), for specific lineage differentiation(Delorme et al. 2006; Dissanayaka et al. 2015). For bone tissue regeneration, differentiation of stem cells into multiple lineages such as osteoblast and endothelial seek cell-specific microenvironment in the hydrogel system (Mao et al. 2016; Seebach et al. 2010). As an example, MSCs differentiate into osteoblastic lineages more robustly in stiffer biomaterials (Mao et al. 2016; Park et al. 2011), whereas they differentiate into endothelial lineages in softer materials (Wang et al. 2013). Human adipose-derived (hADMSCs) co-cultured with hepatocyte-derived cells promoted liver-specific functions of the hepatocytes (Wang et al. 2016). Conversely, endothelial cell populations require more compliant materials to remodel their microenvironment to promote vasculogenesis (Wang et al. 2013; Wood et al. 2010). The multilineage potential of hUCMSCs provided a strong rationale for their use in stem cell-based bone regenerative therapy (Shetty et al. 2010; Wang et al. 2019). Moreover, the soluble factors or biochemical cues (such as growth factors) are one of the important components of such microenvironments and their spatial/temporal concentration is important for cell fate determination (Keung et al. 2010, 2011). Thus, the co-delivery of two populations of cells such as stem cells and endothelial or multiple phenotypic stem cells for cell differentiation would pave the way for tissue repair. It is also important to provide a microenvironment having the above-mentioned biophysical and biochemical cues for each cell type in a hydrogel system. Current porous hydrogels are limited to control/provide a microenvironment of biophysical and biochemical parameters in the hydrogel matrix for one type of encapsulated cells.

The microenvironmental parameter(s) such as matrix topography and/or matrix porosity plays an important role in cell migration, proliferation, and differentiation (Janson and Putnam 2015). However, in most of the studies on hydrogel matrix, the topographical effect has been confined to the 2D substrate due to the limitations in material fabrication techniques (Li and Kilian, 2015; Santos et al. 2012). Hydrogels with macroporosity, representing engineered 3D materials for topographical variation, have been studied for stem cell proliferation and differentiation into specific lineages for regenerative applications (Haugh et al. 2018). In addition to the topographical signature, macroporous hydrogels modify the transport properties of the cellular microenvironment and affect the stem cell fate (Lutolf et al. 2009; Park et al. 2019).

Different methods including microparticle templating, freeze-drying and gas foaming as well as cross-linking of hydrogel micro-ribbons and microgel assembling have been used to prepare macroporous hydrogel (Lutolf et al. 2009). However, the size scale of pores dictates whether cells experience a pseudo-2D microenvironment with the freedom to spread and migrate or a more confining 3D environment (Roach et al. 2010). Gelatin macromers synthetically modified with methacrylate functionalities mediated macroporous hydrogels have been employed for cell encapsulated porous hydrogel for tissue regeneration (Benton et al. 2009), where temperature-responsive fast dissolution of gelatin leads to in situ pore formation in the hydrogel (Dang et al. 2011). The fast dissolution of gelatin microbeads may lead to a drastic change in the mechanical strength of porous hydrogel. Moreover, the current reported porous hydrogel system is mainly used for instant pore generation and their preparation method (such as water–oil emulsion for gelatin porogen) does not allow porogen as cell carrier microspheres (Hwang et al. 2010).

In this paper, we are reporting microenvironment modulating microbeads to fabricate in situ porous hydrogel matrix with two distinct cellular microenvironmental niches. This provides tailorable matrix mechanics, degradation, porosity, and chemical cues/cell–cell interaction within microbeads and in the hydrogel matrix. Furthermore, the electrospraying method of microbead preparation allows encapsulation of the cells into microbeads along with other types of cells in the hydrogel matrix for heterotypic cell function. Electrospraying microbeads made up of various binary mixtures of pectin and gelatin were used to tailor biophysical/biochemical properties of microbeads, which was further mixed with alginate as model hydrogel system, for in situ porous hydrogel matrix. With this system, we can target various heterogeneous tissue repair including bone, skin, periodontal region, etc.

We hypothesized that tailoring the biophysical/biochemical microenvironmental parameters of microbeads in the alginate hydrogel would modulate the microenvironment to instruct stem cells for enhanced cellular function and differentiation. To prove our hypothesis, we have characterized different microenvironmental parameters of microbead and alginate hydrogel, for osteogenic differentiation of human umbilical cord mesenchymal stem cells (hUCMSCs) in the alginate hydrogel loaded with nanosilicate platelets microbeads. Moreover, our microenvironment modulating microbead-hydrogel system provides a novel platform to encapsulate two types of cells in a hydrogel system where each cell is surrounded by a distinct biophysical/chemical

niche to instruct heterotypic cell function and multicellular tissue regeneration. To the best of our knowledge, we are the first to report such a novel hydrogel system for potential heterogeneous tissue regeneration.

Materials and methods

Materials

Sodium alginate (powder, from brown algae) and Gelatin (powder, from porcine skin, Type A Bloom strength 175), Bovine serum albumin (BSA), β-glycerophosphate, ascorbic acid (AA), dexamethasone, formaldehyde, Triton-X 100, FITC albumin, alizarin red S, Oil-O Red, and para-nitrophenyl phosphate substrate with glycine buffer, ALP-BCIP®/NBT, LM Pectin (citrus peel) were purchased from Sigma-Aldrich, USA. Laponite XL21 was received as a gift sample from BYK, USA. Minimal essential medium–alpha modification (alpha MEM), fetal bovine serum (FBS), Trypsin–EDTA, antibiotics, fluorescein diacetate (FDA), propidium iodide (PI), Alamar blue and Phalloidin were procured from Invitrogen, USA, BCA Protein Assay Kit was purchased from Thermo Fisher Scientific, USA. Glacial acetic acid and calcium chloride were purchased from SRL, India. DAPI and Alcian Blue were procured from Alpha Aesar, USA. The filter paper was purchased from Millipore. For all experiments, Milli-Q water was used. All chemicals were used without any modifications. All the organic solvents and chemical reagents used were of analytical grade.

Preparation of pectin-gelatin microbeads

Pectin (P) and pectin-gelatin (PG) blended solutions of 2% and 3% (w/v) were prepared by dissolving in deionized water. The variable ratio of pectin and gelatin (1:1, 2:3, and 1:4 abbreviated as P1G1, P2G3, and P1G4, respectively) were constantly stirred for 4 h. The blended solution was used to prepare microbeads by electrospraying method. In this process, 10 mL of pectin and pectin-gelatin blended solution were electrosprayed into 50 mL of calcium chloride solution (200 mmol L^{-1}) through a stainless-steel needle by varying voltage from 7.0 to 10.0 kV with a pressure of 0.94 bar at room temperature.

Preparation of laponite loaded microbeads

Pectin (P) and pectin-gelatin (PG) blended solutions of 2% and 3% (w/v) were prepared by dissolving in deionized water. The variable ratio of pectin and gelatin (1:1, 2:3, and 1:4 abbreviated as respective P1G1, P2G3, and P1G4) were prepared as described earlier. Later laponite [0.5% (w/v)] was added to the pectin and pectin-gelatin blended polymer solution and stirred overnight for 24 h. Laponite-loaded pectin and pectin-gelatin (L-P, L-P1G1, L-P2G3, and L-P1G4) microbeads were then prepared using electrospraying method. In this process, 10 mL of laponite containing pectin and pectin-gelatin blended solution were electrosprayed into 50 mL of calcium chloride solution (200 mmol L^{-1}) through a stainless-steel needle at a voltage of 10.0 kV and pressure of 0.94 bar to obtain laponite loaded microbeads.

Preparation of P-G microbeads loaded alginate hydrogel.

Pectin (P) and pectin-gelatin (PG) blended microbeads (200 mg) were mixed with 3% alginate (250 μL) solution. The alginate hydrogel (Alg) was prepared and crosslinked with calcium chloride solution (200 mmol L^{-1}) in Teflon mold (height: 2.0 mm, diameter: 10.0 mm). The microbeads encapsulated hydrogel system was further characterized for degradation, porosity, swelling behavior and rheology studies (Supplementary data).

Size distribution analysis of microbeads

The size distribution was calculated using an optical microscope (Olympus CKX-53) fixed with an ocular and stage micrometer. In all dimensions at least 100 particles in five different fields were inspected. For the measurement of each sample, triplicates were used.

Preparation of BSA loaded microbeads/hydrogel and their release profile

BSA-loaded pectin and pectin-gelatin microbeads were prepared by mixing a known amount of BSA (50 mg) in pectin/pectin-gelatin (1 mL) solution and stirred overnight. The mixture was electrosprayed by using a voltage of 10.0 kV and pressure of 0.94 bar in $CaCl_2$ solution. The freshly obtained crosslinked microbeads were collected and stored carefully. These BSA-loaded microbeads (B-P, B-P1G1, B-P2G3, and B-P1G4 (200 mg) with an average size of 350 μm were later mixed in 3% sodium alginate (250 μL) and crosslinked in Teflon mold (height: 2.0 mm, diameter: 10.0 mm) using $CaCl_2$. Similarly, BSA (50 mg) was also loaded into 3% sodium alginate solution (1 mL), and mixed with microbeads prepared without BSA to make matrix-loaded BSA hydrogel. For release study, BSA-loaded hydrogels (BSA in the matrix or microbead) were placed in a 15 mL capped centrifuge tube containing 8 mL PBS (pH 7.4) and incubated at 37 °C in an incubator shaker at 70 rpm. At defined time intervals (1, 3, 5, 7, and 10 days) of incubation, 4 mL of supernatant from each tube was taken out to measure the concentration of BSA released followed by the addition of 4 mL of fresh PBS to maintain sink conditions.

The BSA concentrations in the supernatants were determined using the Micro BCA protein assay kit. The cumulative BSA-release profile from the hydrogels was calculated.

Isolation of human umbilical cord mesenchymal stem cells (hUCMSCs)

Human umbilical cords were collected from the Wharton's Jelly in cords of healthy babies by an established method after their delivery, which is usually discarded as medical waste from MNR hospital, Sangareddy, after obtaining consent from the patient. Experiments were performed as per the requirements given by the Institutional Ethics Committee (IEC) and Institutional Committee for Stem Cell Research (ICSCR) of the Indian Institute of Technology, Hyderabad. IEC and ICSCR approved the entire experimental procedures associated with hUCMSCs, which include extraction, isolation, culture, and experiments with hydrogels (IITH/IEC/2018/12). At 37 °C, umbilical cord tissue was digested for 1 h, kept for agitation in a solution of 5 mg mL^{-1} collagenase-type 1, then a 25 cm^2 culture flask was used to seed the minced tissue suspensions using Dulbecco's modified eagles' medium (DMEM) for culture, supplemented with 10% fetal bovine serum (FBS), 100 U mL^{-1} penicillin-G, 100 µg mL^{-1} streptomycin and 0.25 µg mL^{-1} fungi zone. Flask was incubated at 37 °C and 5% CO_2 with 90% relative humidity and the medium was changed every 3 days.

hUCMSCs encapsulation into microbeads

Umbilical cord-derived hUCMSCs were grown in Dulbecco's modified eagles' medium supplemented with 10% (v/v) of fetal bovine serum (FBS), and 1% (v/v) of an antibiotic–antimycotic solution, at 37 °C, 90% relative humidity and 5% CO_2 atmosphere. hUCMSCs were encapsulated in pectin and all the binary mixtures of pectin-gelatin solution at a density of 1 million cells/mL. Cells at passage 4 were used for all experiments. The harvested cells were dispersed in pectin-gelatin solution for the electrospray. By applying a voltage (10.0 kV) and pressure (0.94 bar) between the needle and collecting stage, the pectin-gelatin blend polymer solution with cells or without cells were extruded from the needle orifice and split into tiny droplets (Zhang et al. 2019), the droplets fell into the solution of 200 mmol L^{-1} calcium chloride.

Later, cell encapsulated microbeads (C-P, C-P1G1, C-P2G3, and C-P1G4) (average size of 350 µm) were washed thrice in PBS to remove the $CaCl_2$ and transferred to well plates supplemented with DMEM culture medium. The medium was changed every other day until the study was completed. The hUCMSCs loaded PG microbeads (500 mg) were later mixed into 1 mL of 3%Alg hydrogel solution. The microbeads containing alginate solution (200 µL) were transferred to Teflon mold (height: 2.0 mm, diameter: 10 mm) and crosslinked by adding 200 mmol L^{-1} $CaCl_2$ solution on the polymer surface (1 mm film of Alg). To secure the homogeneous matrix formation by uniform crosslinking, we have used an adequate amount of calcium chloride and relatively thin hydrogel as well as post-soaking the hydrogel into $CaCl_2$ solution for 10 min. In this process, $CaCl_2$was added slowly into the Teflon mold with a 21-G syringe to form an alginate hydrogel. After 3 min, the alginate hydrogels containing PG microbeads were soaked in calcium chloride solution for 10 min for further crosslinking. The hydrogel was washed with PBS to deplete an excess amount of $CaCl_2$ (Choi et al. 2012). These hydrogels were later transferred to 48-well culture plates and supplemented with 500 µL DMEM culture medium per well. The medium was changed every alternate day for 1 week. Later, the medium was changed every 3 days. Live/dead assay was performed to test the viability of the cells encapsulated microbeads. All the materials used for cell culture analysis were UV sterilized and performed under a sterile environment (Supplementary data).

hUCMSCs encapsulated into the hydrogel matrix

Alginate solution (3% w/v) was prepared by suspending alginate in PBS (pH 7.4). Deionized water was used to dissolve $CaCl_2$to a final concentration of 200 mmol L^{-1}. A 0.45 µm membrane filter was used to sterilize both the solutions. hUCMSCs were collected from monolayer culture using trypsin–EDTA, centrifuged, and resuspended in the medium at a density of 2×10^6 cells/mL. Passage 4 cells were used for all experiments. Sterile alginate solution was mixed with suspended cells (2×10^6 cells/mL). The PG microbeads (500 mg) were added per 1 mL alginate solution. The cell-containing alginate–PG microbeads solution was then added to the Teflon molds and crosslinked by adding a 200 mmol L^{-1} $CaCl_2$ solution on the polymer surface. After 10 min of crosslinking, hydrogel discs were retrieved and washed with PBS to remove excess calcium. These hydrogels were later transferred to 48-well culture plates and supplemented with 500 µL DMEM culture medium per well. The medium was changed every alternate day for 1 week. Later the medium was changed every 3 days. Live/dead and DAPI staining was performed to determine the viability of cells encapsulated in the hydrogel matrix. Alamar blue assay was carried out to evaluate cell proliferation (Supplementary data).

In vitro osteogenesis assays

For the in vitro osteogenic assays, hUCMSCs were encapsulated into the bulk gel phase (2×10^6 cells/mL) of alginate matrix, by mixing in the polymer solution. Later sacrificial

laponite (having inherent osteoinductive potential) containing L-PG microbeads (500 mg) with an average size of 350 µm were mixed into 1 mL of Alg hydrogel solution and calcium ion crosslinking was performed. After crosslinking, the hydrogels were transferred to tissue culture substrate with DMEM supplemented with 10% Fetal Bovine Serum and 1% penicillin/streptomycin. No additional osteogenic factors were used for the cell culture study. At pre-determined time intervals, alkaline phosphatase (ALP) activity and staining were performed to evaluate the osteogenic behavior of the microbead hydrogel system (Supplementary data).

Statistical analysis

All experiments were performed in triplicate and expressed as mean ± standard deviation. Statistical differences for all the experiments between groups were analyzed using one-way ANOVA with the Tukey post hoc test using Graph Pad Prism software for statistical computation. The groups with a significant difference were represented with symbols to represent the difference (*$P < 0.05$, **$P < 0.01$, ***$P < 0.001$).

Results and discussion

Microenvironments modulating hydrogel platform

Engineering hydrogel microenvironment parameters such as mechanical strength, degradability, cell-adhesive ligand presentation, microstructure, soluble cues, and cell–cell interactions are essential to recapitulate the stem or progenitor cell niche for specific functional tissue regeneration (Wagers 2012). Generation of functional tissues consisting of different types of cells may require a specific microenvironment surrounding for stem cells/progenitor cells to differentiate into specific lineages such as osteoblast and endothelial cells for vascularized bone tissue. Reported porous hydrogel systems can modulate the microenvironment specific to one type of phenotype differentiation which is uniform throughout the matrix (Wang and Chen 2013).

Here, for the first time, we have reported a method to prepare hydrogel, which is capable of modulating the microenvironment parameters specific to dual phenotype differentiation in a single hydrogel system (Fig. 1) as a novel platform for heterotypic cellular tissue regeneration. In this study, we

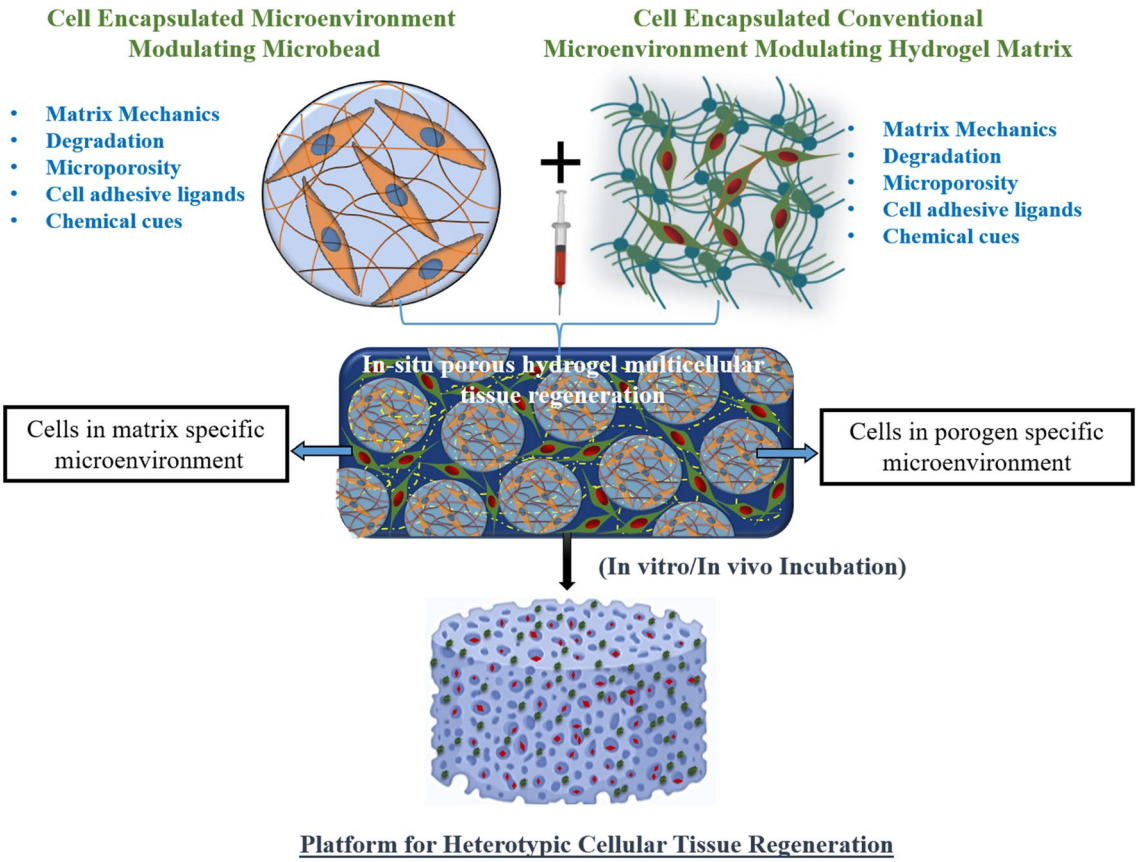

Fig. 1 Schematic representation of tailored microenvironment modulating microbeads and hydrogel system

have created a microbead system using blended-biopolymers (pectin-gelatin or PG) and electrospraying method to tailor physicochemical properties (porosity, degradation, mechanical and chemical cues) and encapsulate cells, respectively, in addition to the conventional microenvironment modulation of hydrogel matrix (Fig. 1). Pectin and gelatin blended in 1:1 ratio are denoted as P1G1, pectin-gelatin in 2:3 ratio as P2G3, and pectin-gelatin in 1:4 ratio as P1G4throughout the paper. In using different concentrations of gelatin (50%, 65%, and 75%) in the pectin-gelatin microbead, we have tailored the degradation of the microbead, and thus porosity to regulate a suitable microenvironment. From our preliminary experiments, we have optimized the gelatin ratio (50%, 65%, and 75%) to achieve a gradual change in the degradation among different microbead systems. Thus, the respective ratio of the pectin-gelatin is used to ensure a porous hydrogel system with controlled degradation and mechanical behavior (Hwang et al. 2010).

We have discussed different microenvironment parameters within microbead and hydrogel matrix. The scaffold shown in Fig. 1 is a pictorial representation of the future platform for heterotopic tissue regeneration encapsulating two types of cells within two distinct microenvironments. In this paper, we have validated the effects of two different microenvironments on the osteogenic differentiation of hUCMSCs encapsulated in the matrix of the hydrogel system.

Microenvironment modulating microbead preparation and encapsulation of stem cells

Microbead preparation with tailored size

Microbeads with tailored chemical (blending of biopolymers—pectin and gelatin) and physical properties (size and degradation) were prepared by electrospraying method (see methodology for details). The effect of different electrospraying parameters such as voltage, flow rate, polymer solution concentration and distance on the size of microbead were studied (Supplementary data and Table 1). Figure 2 shows the variation of the size of pectin (P) and pectin-gelatin (PG) microbeads at different voltages (7–10 kV) while other parameters were kept constant at 1.5 mL min^{-1} flow rate, 10 cm distance, and 200 mmol L^{-1} of $CaCl_2$and at a pressure of 0.94 bar. The electrospraying method resulted in a relatively narrow distribution of microbeads for specific applied voltage, where the average sizes of the microbead can be tuned from 315 to 1500 µm. The average size of the pectin based microbeads decreases from 710 ± 40 µm to 350 ± 10 µm when the applied voltage changes from 7 to 10 kV (Fig. 2a–c). Similar to pectin microbeads, a decrease in the size is observed in PG (1:1, 2:3, 1:4) blended microbeads (Fig. 2d–l). Thereafter, the average size of microbeads changed with varying blend compositions for P1G1—from 710 ± 20 to 340 ± 10 µm (Fig. 2 n), for P2G3—from 770 + 20 µm to 350 + 10 (Fig. 2o) and P1G4—from 775 ± 20 to 350 ± 20 µm (Fig. 2 p) when the applied voltage increases from 7 to 10 kV. This size distribution data proves the narrow size distribution of microbeads (Fig. 2m-p). Similar to the electrospinning method, a decrease in particle size with increasing applied voltage results from the stretching of polymer solution due to charge repulsion within the polymer (Thompson et al. 2007). The flow rate of the polymer solution at constant voltages and other electrospraying parameters affects the shape of pectin-gelatin microbeads slightly, thus, the flow rate of more than 1.5 mL min^{-1} results in cone-shaped microbeads (Figure S2, Supplementary data). At constant voltage, the increase in flow rate resulted in faster release of stretched polymer microbeads from the needle tip to crosslinking solution before recovery to spherical shape. The effect of other electrospraying parameters such as the concentration of polymer solution, $CaCl_2$ concentration, and the distance between the nozzle-collector on microbead size-shape are shown in the supplementary information (Figure S1, S2, S3, Supplementary data). 200 mmol L^{-1} $CaCl_2$ concentration and 10 cm distance between nozzle tip-to-collector were found optimum at a constant voltage of 10 kV and 1.5 mL min^{-1} of flow rate. Similarly, increasing the concentration of pectin and calcium chloride solution tends to make the microbeads more spherical and uniform (Figure S1, S2, S3, Supplementary data). However, the concentration of the polymer solution of 2% pectin, 3% gelatin is desired to acquire optimum viscosity and results in spherical-shaped microbeads when other electrospraying parameters are kept constant at their optimum values. Note that electrospraying with optimized parameters such as 10 kV, 10 mL min^{-1}, 2–3% polymer solution, and 10 cm distance result in uniform sacrificial microbeads (350 µm size) and have been used for other studies such as encapsulation of cells and fabrication of microbead loaded hydrogels. The crosslinking of P and PG microbeads by Ca^{2+} ions was due to ionic interactions between Ca^{2+} and carboxylic groups of galacturonic blocks of the pectin chain.

Stem cells (hUCMSCs) encapsulated microbeads

hUCMSCs were used as model cells to encapsulate into the microbeads using the electrospraying method in a sterile environment. As expected from previous reports (Gryshkov et al. 2014; Xu et al. 2019), lower voltage (below 10 kV) mediated electrospraying process did not result in noticeable cell death in the process of hUCMSCs cell encapsulation into pectin/pectin-gelatin microbeads (Figure S4, Supplementary data). Moreover, significant cell proliferation was observed upon culturing of hUCMSCs encapsulated microbeads for 7 days.

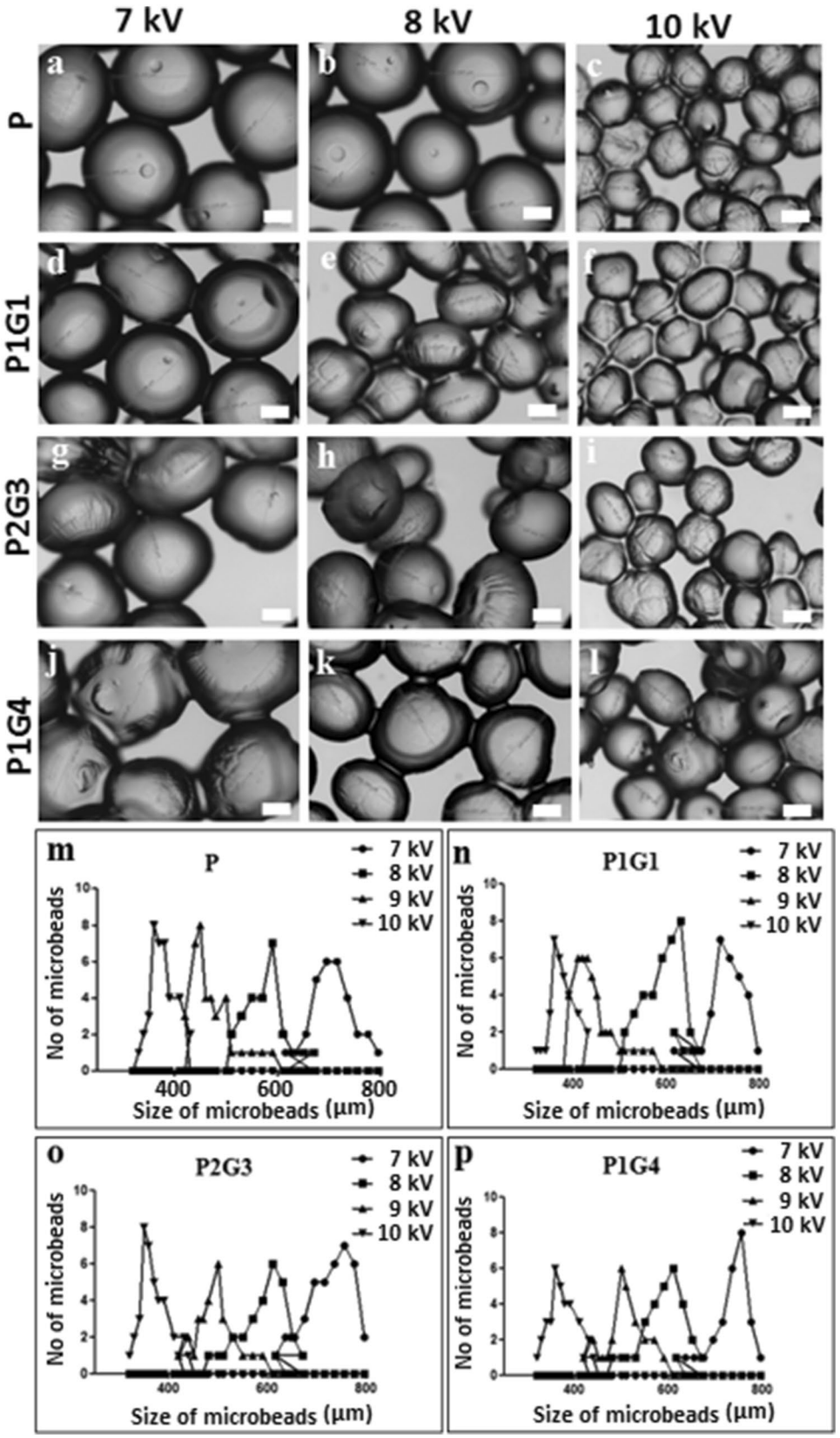

Fig. 2 Optical microscopy images of microbeads displaying the effect of applied voltages (**a**–**l**) on the morphology of the P (**a**–**c**), P1G1 (**d**–**f**), P2G3 (**g**–**i**), P1G4 (**j**–**l**) microbeads at a flow rate of 10 mL min^{-1}, 2% pectin,3% gelatin polymer solution and a distance of 10 cm between nozzle and collector. The size distribution analysis plot of different microbeads, P (**m**), P1G1 (**n**), P2G3 (**o**), and P1G4 (**p**) microbeads. Over 100 microbeads of each sample were measured to plot size distribution curve. Scale bar is 200 µm

Microbead encapsulated porous hydrogel system

Tailored degradable microbeads with/without cells were used to make a hydrogel system consisting of two unique microenvironments, namely conventional bulk hydrogel matrix (alginate as a model system) and microbead matrix (Fig. 1). Different physicochemical properties such as porosity, swelling behavior, degradation and mechanical properties of the hydrogel were evaluated. The hydrogel microstructure, porosity and swelling behavior are depicted in Fig. 3. Micron-scale porosity formation within the hydrogel matrix mediated by tailored degradable microbeads before and after 7 days of degradation was evaluated by scanning electron microscopy (Fig. 3a–j). The cross-section of alginate hydrogels loaded with pectin (P) microbeads show the presence of microbeads even after 7 days of degradation (Fig. 3g), whereas the pectin-gelatin-blend (PG) microbeads-loaded hydrogel resulted in a porous structure with interconnected pores (Fig. 3h–j). Moreover, higher gelatin containing microbeads i.e., P1G4 loaded alginate hydrogels resulted in higher porous microstructure as shown in Fig. 3j. Similarly, pore size can be altered by tailoring microbead size with varying electrospraying parameters or by changing the pectin-gelatin composition ratio.

The porosity of the hydrogel after 7 days of incubation in PBS at 37 °C was determined and depicted in Fig. 3l. The porosity of the microbeads-loaded hydrogel increases with the amount of gelatin, thus hydrogel with microbeads of P, P1G1, P2G3, and P1G4 resulted in 12%, 18%, 25%, 38%, and 45% porosity, respectively. It was also observed that the rate of hydrogel degradation is affected by the ratio of the concentrations of the polymer and the crosslinker used. It was previously reported that the ratio of alginate to pectin influences the gel strength and the swelling properties (Vaziri et al. 2018). Alginate along with pectin with a low degree of methoxyl substitution (DM) has higher stability due to the higher degree of crosslinking (Günter et al. 2020). Hence, plain alginate with a relatively lower polymer concentration had less swelling ratio. Note that no significant pore formation occurred in the hydrogel matrix during the flash-freezing and freeze-drying process which is further confirmed from the porosity (from SEM image and percentage of porosity) in the hydrogel system without microbeads (Shapiro and Cohen 1997). The increase in the porosities is attributed to the faster degradability of the microbeads with a higher amount of gelatin at 37 °C associated

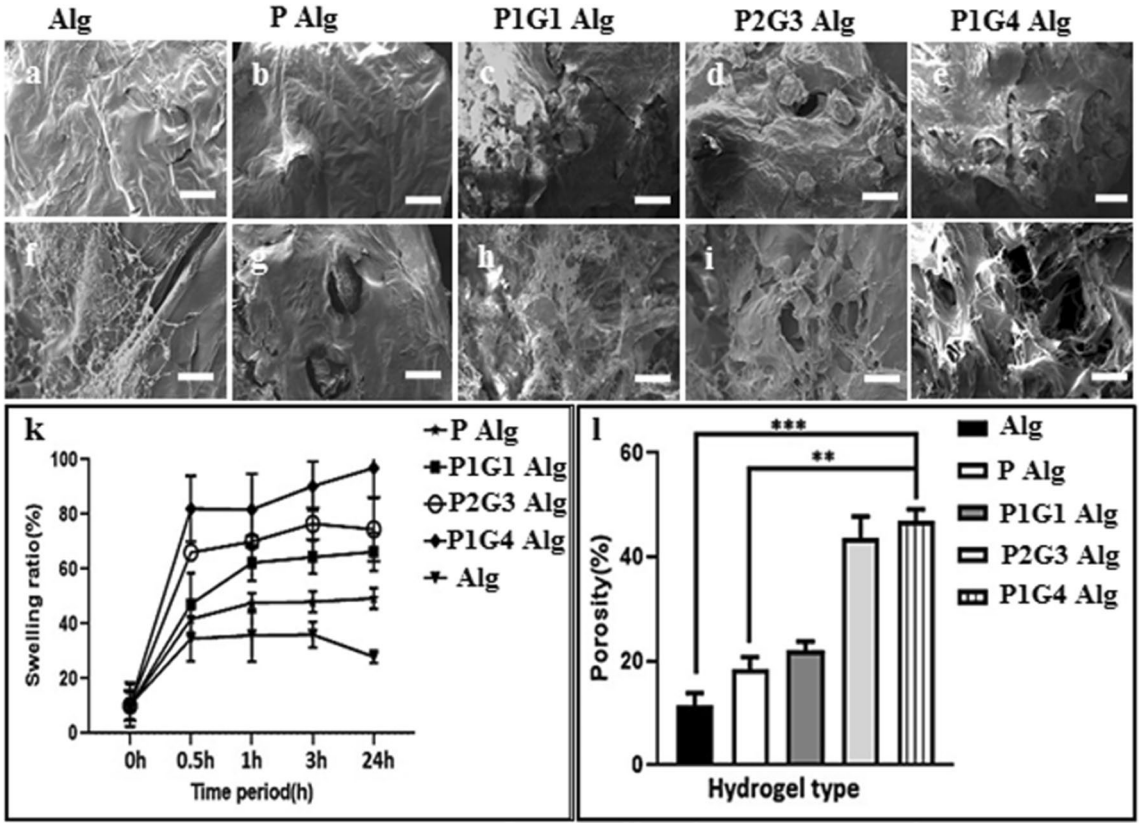

Fig. 3 Cross-sectional SEM image of hydrogels (**a**–**e**) before incubation in PBS and hydrogels (**f**–**j**) after 7 days of incubation in PBS at 37 °C. Result of swelling ratio (%) of Alg, P, P1G1, P2G3, and P1G4 microbeads loaded in alginate hydrogel (**k**). Result of the porosity of different microbeads-loaded hydrogels (**l**). (*$P < 0.05$, **$P < 0.01$, ***$P < 0.001$). Scale bar is 100 µm

with gelatin gel-to-sol phase transformation (Sakai et al. 2009) (details are in the following section). Porosity within the hydrogels is important for the exchange of nutrients, oxygen, fluid, cell migration and cellular crosstalk which helps in cellular proliferation and differentiation (Loh and Choong 2013). Moreover, suitable porosity is required to facilitate optimal attachment, proliferation, and differentiation which depends on the cell types and target tissue (Muschler et al. 2004). Recent studies revealed that bone cells show higher adhesion and optimum attachment in the scaffold with 120–130 µm pore size (Lee et al. 2008) whereas another study reported that collagen/glycosaminoglycan (CG) scaffolds with 325 µm porosity scaffold resulted in higher proliferation(Murphy et al. 2010). Hence, the development of hydrogel with controlled and tailored porosity is essential to create an optimum 3D microenvironment specific to cells and tissue. The electrosprayed PG blended microbead template system is unique method to make hydrogel with optimum pore size and porosity specific to each cell type. The effect of the hydrogel porosity and 3D microenvironment on the cell viability, proliferation and differentiation of encapsulated hUCMSCs were evaluated and described here in the following section.

The swelling capability represents the water absorption capacity of the hydrogel system. The swelling properties (%) of the different microbeads loaded alginate hydrogels in PBS (pH 7.4) are shown in Fig. 3k. Hydrogels with PG microbeads show a higher swelling ratio (60% to 85%) compared to 30% for hydrogel without microbeads (Alg), which increases from 45% with pectin (P) microbeads hydrogel to 85% with pectin-gelatin (P1G4) microbeads hydrogel. Moreover, for all hydrogel systems swelling equilibrium reached within 30 min, demonstrating the sponge-like characteristics of these hydrogels (Costantini et al. 2015). The swelling properties of the hydrogel matrix depend on several factors, mainly the hydrophilicity of the polymer network, the nature of bonding (crosslink), and their density (Buwalda et al. 2014; Gupta et al. 2002; Santoro et al. 2014). As these hydrogels are made up of an alginate matrix with a similar crosslinking-network, one can expect that the variation in swelling properties among these hydrogels are mainly from the loaded microbeads. The higher swelling properties of hydrogel with microbeads of pectin and pectin-gelatin are likely due to the higher hydrophilic properties of pectin/gelatin, and a decrease in the network crosslink (Ca^{2+} bridging) density in the microbeads with increasing gelatin content (Young et al. 2005).

Modulation of microbeads mediated microenvironment

Tailored degradation of microbeads

Tailor degradation with specific porosity is necessary to create a unique 3D microenvironment surrounding encapsulated cells in the hydrogel system (Marklein and Burdick 2010). Figure 4 shows the morphological changes (Fig. 4a–d) and quantitative degradation (%) of different microbeads in Fig. 4i. The optical microscopy images of different microbeads before (Figure S7, Supporting Information) and after 7 days (Fig. 4a–d) of degradation indicate the presence of spherical pectin (P) microbeads even after 7 days whereas, significant degradation (decrease in microbeads numbers and size) is observed for pectin-gelatin blended (PG) microbeads. Moreover, the extent of degradation increases with gelatin concentration, which is further supported by the degradation percentage (Fig. 4i). The microbeads, P, P1G1, P2G3, and P1G4 show each respective degradation at 11%, 49%, 64%, and 79% on day 3, which further degraded to 29%, 82%, 87%, and 92% on day 5. It is also inferred from the degradation (%) plot that almost complete degradation is observed for gelatin blended microbeads P1G1, P2G3, and P1G4 by day 7, Fig. 4i. Enhanced degradation of PG microbeads is associated with the dissolution of gelatin at 37 °C at a higher pace than pectin galacturonic chains dissolution (van den Bosch and Gielens 2003). These PG blended microbeads could be used as microbeads with tailored degradation time for 3D microenvironment modulation in different hydrogel matrix systems for various tissue regeneration applications.

Degradation of microbeads in the hydrogel matrix

The degradation behavior of different microbeads in the hydrogel (alginate) was studied to evaluate their degradability in the hydrogel matrix using fluorescence imaging and degradation (%) study, depicted in Fig. 4e–h. Autofluorescence from the pectin-gelatin polymer was used to probe the degradation of the microbeads in the alginate hydrogel matrix. On day 1, the microbeads are visible (bright contrast) in the matrix of alginate hydrogel (Figure S7e-h, Supplementary data), which changes to a relatively darker spot by day 7 of their degradation (Fig. 4f–h) showing the formation of pores in the hydrogel matrix. The intact P microbead morphology is clearly visible in the hydrogel's matrix (Fig. 4e), whereas, the radiolucent porous area is visible in P2G3/P1G4 loaded hydrogels on day 7 (Fig. 4g, h). As expected, the extent of degradation of microbeads and the associated pore formation depends on the faster dissoluble gelatin content in the microbeads. This observation is further supported by the reduction in the total fluorescent signal in the different hydrogel systems after 7 days of degradation (Fig. 4k), which is minimum for P-hydrogel and maximum for P1G4microbeadhydrogel. Figure 4j shows the degradation percentage of the microbeads loaded hydrogels during incubation in PBS (pH 7.4) at 37 °C. Thus, P, P1G1, P2G3, and P1G4 loaded hydrogels result in 29%, 62%, 65%, and 66% degradation, in the stated order, by day 5,

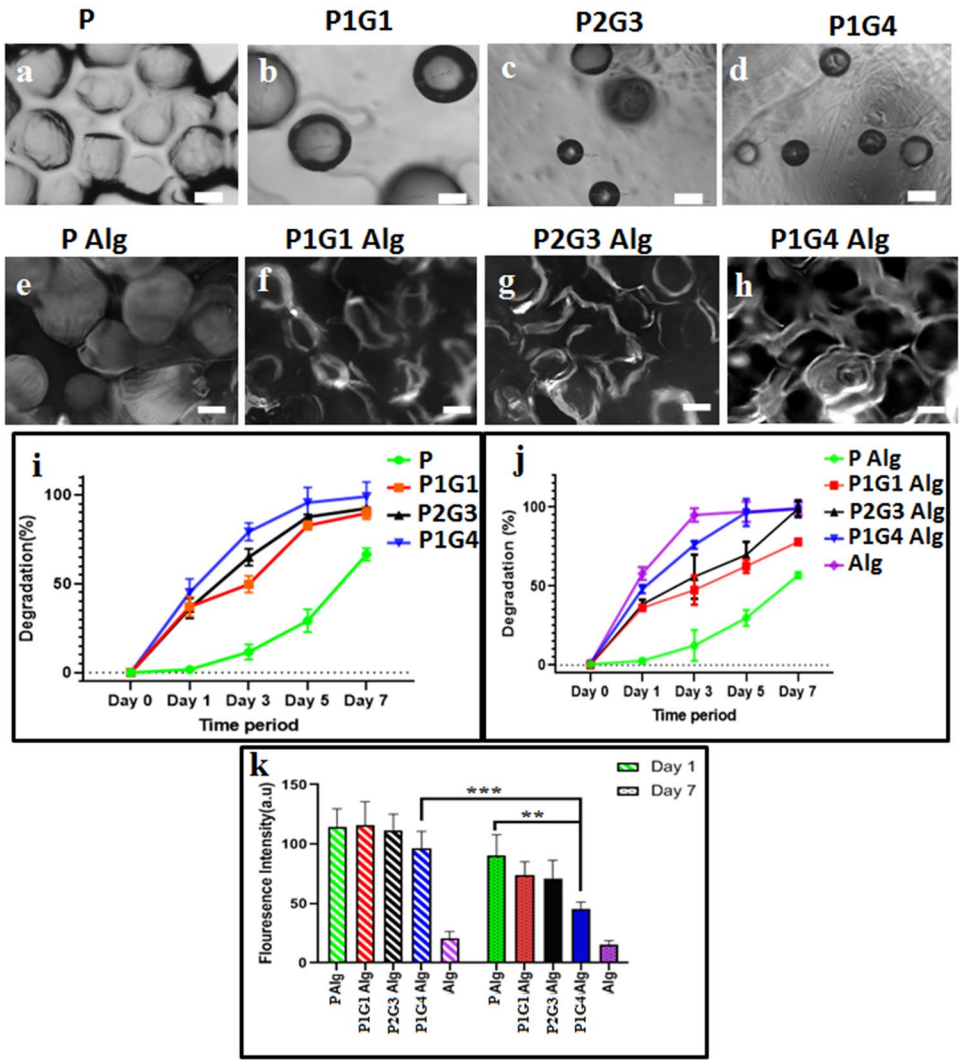

Fig. 4 Optical microscopy images of P (**a**), P1G1 (**b**), P2G3 (**c**), and P1G4 (**d**) microbeads after 7 days degradation. Fluorescence microscopy images of Alg hydrogel loaded with P (**e**), P1G1 (**f**), P2G3 (**g**), and P1G4 (**h**) microbeads on day 7. Degradation (%) graphs of microbeads (**i**) and microbeads loaded Alg hydrogels (**j**) over an interval of 7 days. The quantification of the fluorescence intensity (**s**) of the hydrogels is calculated by capturing 25 images of each hydrogel using image intensity analysis Axiovert software of the fluorescence microscope. (*$P < 0.05$, **$P < 0.01$, ***$P < 0.001$). Scale bar is 200 µm

which further increased to 53%, 68%, 75%, and 79% after 7 days of degradation, correlating well with the fluorescence imaging data above. When the calcium crosslinked alginate matrix was incubated in PBS, Na + ions present in the PBS medium enter the matrix and undergo ion exchange with Ca^{2+} ions, which were attached to –COO– groups of mannuronic (M) blocks of the matrix. This results in the relaxation of M chains. Later, the external Na^{+} ions enter into 'egg-box' cavities of the matrix and replace the already existing Ca^{2+} ions (Kikuchi et al. 1999). The fully hydrated alginate structure begins to lose its structural integrity due to the disruption of 'egg-box' cavities causing the disintegration of the matrix into big chunks, followed by complete dissolution of the matrix. Hence the degradation of these alginate hydrogels occurs due to the disintegration of matrix networks and breakage of the crosslinking bonds. The difference in the degradation behavior between the alginate and PG microbead containing alginate hydrogel might be due to the amorphous and semi-crystalline nature of the alginate and pectin polymer, respectively. (Georget et al. 1999; Gohil 2011). It was also reported that calcium alginate beads do not exhibit good stability in the physiological fluid such as phosphate buffer at pH 7.4 (Bajpai and Sharma 2004). The presence of counter ions in the swelling medium induces an ion exchange with cross-linked Ca^{2+} ions that are present within the 'egg-box' bridging network and results in the degradation of alginate beads within few hours (Bajpai and Kirar 2016).

Alginate hydrogels showed higher degradation compared to alginate hydrogels loaded with PG microbeads as alginate mixed with pectin and PG microbeads has reduced gel shrinkage due to syneresis during the gel formation process(Ramdhan et al. 2020; Walkenström et al. 2003). P1G4Alg, which consists of high gelatin concentration, degrades faster compared to others. The microbeads degradation in the hydrogel matrix is similar to their uncapsulated form (Fig. 4a–d). Important to note that the cell-encapsulated PG microbeads can modulate the microenvironment

of the hydrogel by tailoring the porosity/degradability in the microbeads, choosing microbeads with suitable percent of gelatin blend as required for specific cells/tissue remodeling time. Moreover, conventional hydrogel-associated microenvironment can be further modulated by the use of a suitable hydrogel system (instead of alginate matrix) in addition to microbeads associated 3D microenvironment (porosity/degradation) modulation.

Chemical cues

BSA, as a model chemical cue, was encapsulated into the microbeads or hydrogel matrix and its release profile was probed from BSA-microbeads encapsulated hydrogel and hydrogel (BSA directly encapsulated in the hydrogel matrix) (Fig. 5). BSA released from all microbeads shows sustained release with an initial 20% release at 24 h. Moreover, BSA from B-P1G4 is observed to be almost 100% release on day 10 compared to ~ 80% for B-P, B-P1G1, B-P2G3 microbeads. The BSA release from the microbeads, when encapsulated into the alginate hydrogel matrix, shows a sustained release profile, but the total release on day 10 decreases to 55%, 50%, 45%, and 40% from B-P1G1, B-P2G3, B-P1G4, and B-P microbead-hydrogel, respectively, with a relatively lower initial release (10%) at 24 h (Fig. 5a). The slower release of BSA from microbeads through hydrogel matrix compared to their release from microbeads suspension in PBS (pH 7.4). This is due to the presence of a possible diffusion barrier of the alginate matrix and lower BSA release from Alg hydrogel as the hydrated structure loses its structural integrity in PBS due to disruption of 'egg-box' cavities and the alginate chains. Hence, BSA entrapped within the alginate chains could not be released out into the medium due to alginate hydrogel structural disorganization. Alginate

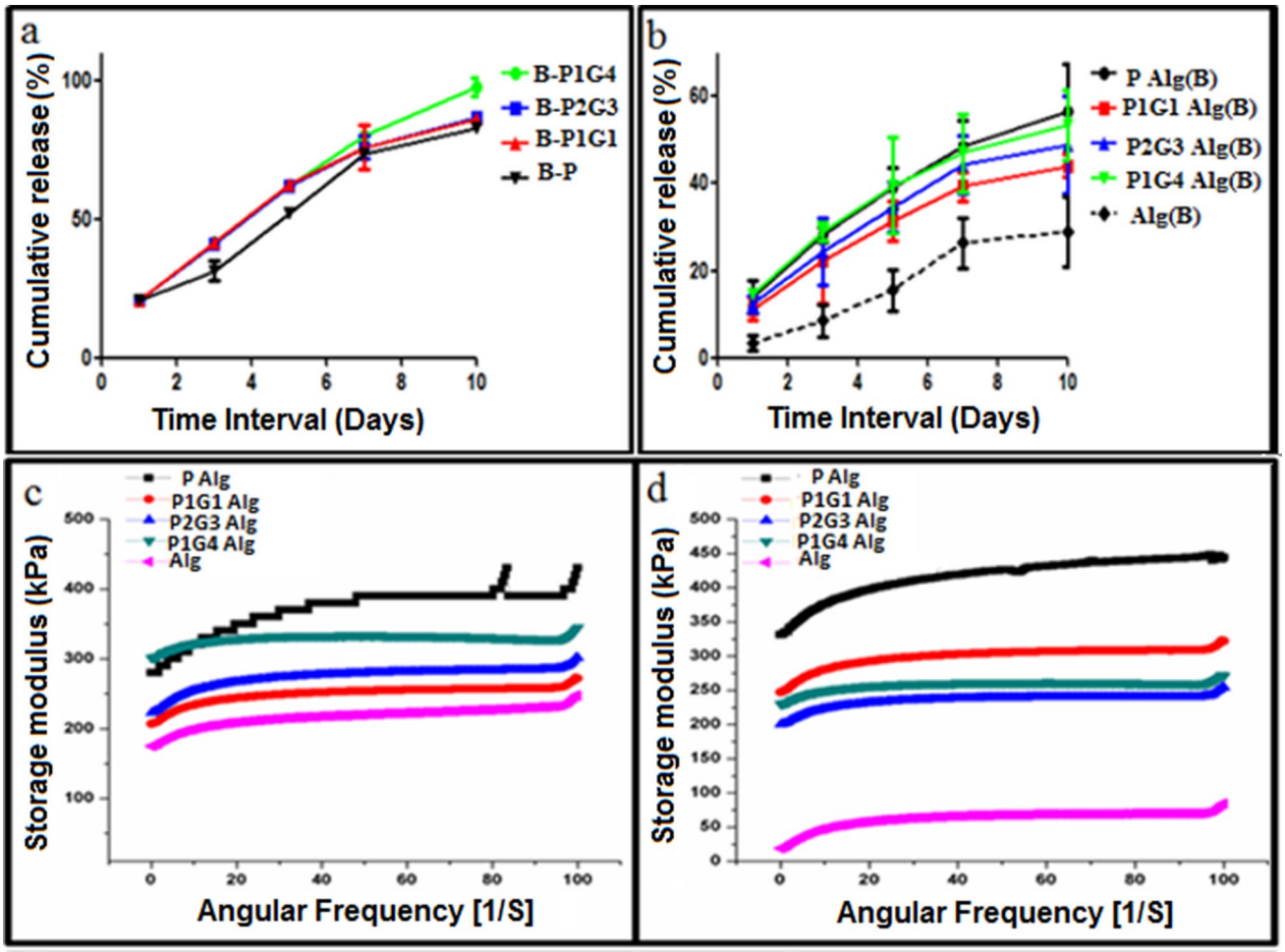

Fig. 5 In vitro BSA release profile of hydrogel with B-P, B-P1G1, B-P2G3, and B-P1G4 loaded microbeads (**a**), in vitro release from BSA loaded Alg matrix loaded with microbeads [PAlg(B), P1G1Alg(B), P2G3Alg(B), and P1G4Alg(B)] (**b**) was evaluated in triplicates at 37 °C for 10 days. Frequency sweep analysis visualizing the storage modulus (G′) within a range of angular frequency. Graphs shows (G′) values of Alg and Alg hydrogels loaded with P, P1G 1, P2G3, and P1G4 microbeads before degradation (**c**) and after degradation (**d**) by dissolving in PBS for 7 days at 37 °C

which is a hydrophilic polysaccharide during degradation results in pH variations (as its matrix gets dissolved), carboxylate groups in the alginate backbone become protonated during degradation and forms hydrogen bonds (Lee and Mooney 2012). This change in pH would have resulted in agglomeration or precipitation of BSA (Estey et al. 2006), led to retarded BSA release (Norudin et al. 2018). Similarly, the higher release of BSA from microbeads with maximum gelatin (B-P1G4) is associated with the faster degradation of gelatin within the hydrogel matrix or in PBS suspension (Figs. 4i, 5a). A significant difference was observed in BSA release at day 10, B-P1G4 microbeads loaded in hydrogel showed 97% release and 55% from the Alg(B) matrix loaded with P1G4 microbeads. This difference in the release profiles from two distinct places: hydrogel matrix and microbead matrix, within a hydrogel system provides a unique platform to encapsulate multiple chemical cues (protein, growth factors, drug, etc.) and can tailor their concentration to create two distinct 3D microenvironments. Thus, one can encapsulate specific chemical cues such as growth factors or drug molecules within the alginate hydrogel matrix for slower release and other chemical cues within the sacrificial PG microbeads for relatively faster release.

Mechanical properties

Hydrogels exhibit a storage modulus (G') higher than the loss modulus (G''), denoting the elastic character of hydrogels and their gel state. Frequency sweep (within the viscoelastic region 0.1 to and 10 rad s^{-1}) of with/without microbeads-encapsulated alginate hydrogels were performed to check the storage modulus (G') of the hydrogels before and after 7 days of incubation in PBS (pH 7.4) and depicted in Fig. 5c, d. The storage modulus values of hydrogel increased significantly with the addition of microbeads in the hydrogel which may be due to the presence of pectin and their possible involvement in the crosslinking between microbead surface and alginate matrix (Toft et al. 1986). However, the order of storage modulus of hydrogel with different microbeads is yet to be understood clearly and needs a more detailed study in the future. The storage modulus (G') values for plain alginate hydrogels (without microbeads) before and after incubation in the PBS are 225 kPa, and 50 kPa. Similarly, storage modulus values of the P, P1G1, P2G3, and P1G4 microbeads-loaded hydrogel before degradation is 420 kPa, 265 kPa, 275 kPa, and 305 kPa, respectively, and after degradation, it is 445 kPa, 275 kPa, 245 kPa, and 250 kPa. Interestingly, microbead encapsulated hydrogels show a limited decrease (< 15%) in their storage modulus after degradation (7 days) compared to alginate hydrogel without microbeads (75% reduction). Note that 7 days incubation in PBS results in more than 80% degradation of microbeads. The exact reason for such superior mechanical properties of P, P1G1microbead mediated porous-alginate hydrogel is yet to be investigated. Nonetheless, this may attribute to the formation of possible macromolecular bridging of pectin and gelatin with alginate matrix through hydrogen bonding and ionic crosslinking of pectin and alginate polymer chains (Alonso-Mougán et al. 2002; Ching et al. 2008). It was reported that a dotting mode of egg-box structure formation in the alginate hydrogel matrix occurs during calcium crosslinking (Donati et al. 2006). Suitable mechanical properties of the hydrogel are essential for cell adhesion, migration, proliferation, and differentiation. Reported porous hydrogels with gelatin microbeads show the major disadvantage of fast deprived mechanical properties due to the quick dissolution of gelatin-microbeads at 37 °C (Sokic et al. 2014). Porosity in hydrogels drastically changes the mechanical properties. Conversely, this tailored degradable pectin/pectin-gelatin microbeads- loaded alginate hydrogels result in small changes in their mechanical properties even after complete dissolution of microbeads in a porous hydrogel, which can be further tuned using suitable microbead composition. The minimal change in the modulus values of P2G3/P1G4-hydrogels after degradation of microbeads (245/250 kPa), slight elevation in modulus of P (445 kPa) and P1G1 hydrogel (275 kPa) after degradation might be due to higher pectin composition compared to pure alginate hydrogels (50 kPa) emphasizes that the PG microbeads improve the mechanical properties of hydrogels with ~ 50% porosity (Fig. 3l).

Stem cell encapsulated microbead and cross-talk with cell in the hydrogel matrix

The PG microbeads provide a unique microenvironment as discussed above. Cells (hUCMSCs) encapsulated microbead system was loaded into the hydrogel matrix and the proliferation of stem cells in the microbead microenvironment was investigated (Fig. 6) using microscopy. The fluorescence images and optical images of hydrogels clearly show the presence of spherical microbeads (C-P, C-P1G1, C-P2G3, C-P1G4) in the hydrogel matrix (Fig. 6). The cells (seen as a green dot) are distinct within microbead (microbead-loaded hydrogel, Fig. 6l–o) and cells encapsulated within the hydrogel matrix (alginate hydrogel without microbeads in Fig. 6k, p). On day 1 most of the cells are appear as a dot within the microbeads or the matrix. However, on day 7, as expected, the spherical microbeads encapsulated with the cells were still visible in PAlg hydrogel. Conversely, in gelatin blended microbeads, C-P2G3, and C-P1G4 loaded hydrogel showed spreading of cells within the non-spherical microbead matrix, indicating the dissolution of microbeads. In addition to the abovementioned cell confinement/spreading in the different hydrogels, cells in all microbead matrix were viable (green fluorescein diacetate to stain live cells

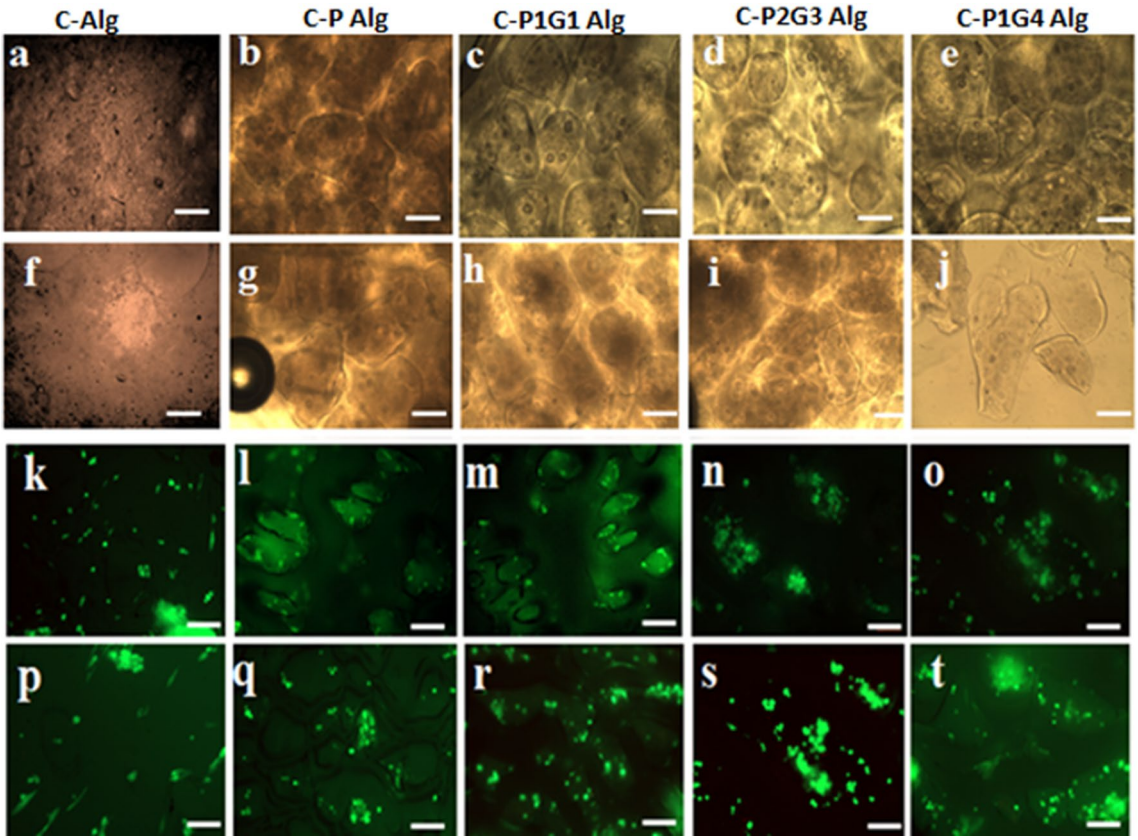

Fig. 6 Optical microscope images of cells encapsulated PG microbeads loaded in alginate hydrogel (**a**–**j**) before degradation (**a**–**e**) on day 1 and after degradation (**f**–**j**) on day 7. Fluorescence microscope images show live dead assay result of the viable cells encapsulated within the microbeads (**k**–**t**) before degradation (**k**–**o**) on day 1 and after degradation (**p**–**t**) on day 7. Scale bar is 100 μm

and red propidium iodide for dead cells staining) at day 1 and 7. However, few dead cells were also observed but they appeared to be less in comparison to live cells with less fluorescence intensity. Moreover, as expected, there was a significant increase in the cell numbers as colonies at the periphery of degrading microbeads in the C-P1G2, C-P2G3 and C-P1G4 hydrogels, indicating significant migration and proliferation of the encapsulated cells (Fig. 6r–t) compared to fewer cell numbers in C-Phydrogel and alginate hydrogel (Fig. 6p). These results indicate that the encapsulated hUC-MSCs maintained their viability within the microbeads and controlled the 3D microenvironment such as degradation of microbeads, thereby allowing cellular migration and proliferation within the microbead confinement.

Porous hydrogel for bone tissue regeneration

Porous hydrogels containing laponite-loaded microbeads were evaluated for bone tissue regeneration using hUC-MSCs as a model for tissue regeneration. Fluoride doped laponite nanosilicate have been reported for superior osteogenic properties in our previous publication (Veernala et al. 2019). We hypothesize that further encapsulation into our PG microbeads may provide a unique microenvironment for stem cell (in hydrogel matrix) proliferation and osteogenic differentiation for bone tissue regeneration. Figure 7 shows the cells in different hydrogels matrix during the culture for 10 days. Cell encapsulated into the alginate matrix of different hydrogels results in homogenous cell distribution throughout the alginate matrix (green and blue dot) at day 1, Fig. 7a, f, k, p. The fluorescence images of hydrogels with laponite containing L-PG microbeads (L-P1G1, L-P2G3, and L-P1G4) show spherical lacunae at day 7 of their culture associated with the degraded microbeads (Fig. 7h–j) as described before compared to the presence of microbeads in pectin (L-P) microbead hydrogel (Fig. 7g). However, cell nucleus count (blue stained by DAPI) and cells (green dots stained by fluorescein diacetate) in the L-PG microbeads hydrogels were observed to increase during culture of hydrogels for 10 days or more, indicating higher proliferation of cells, and their spheroids formations in the porous hydrogels (Figs. 7s, t, x, y) compared to L-P microbeads or without microbead alginate hydrogels (Figs. 7g, p, q). This observation is further supported by the Alamar Blue proliferation

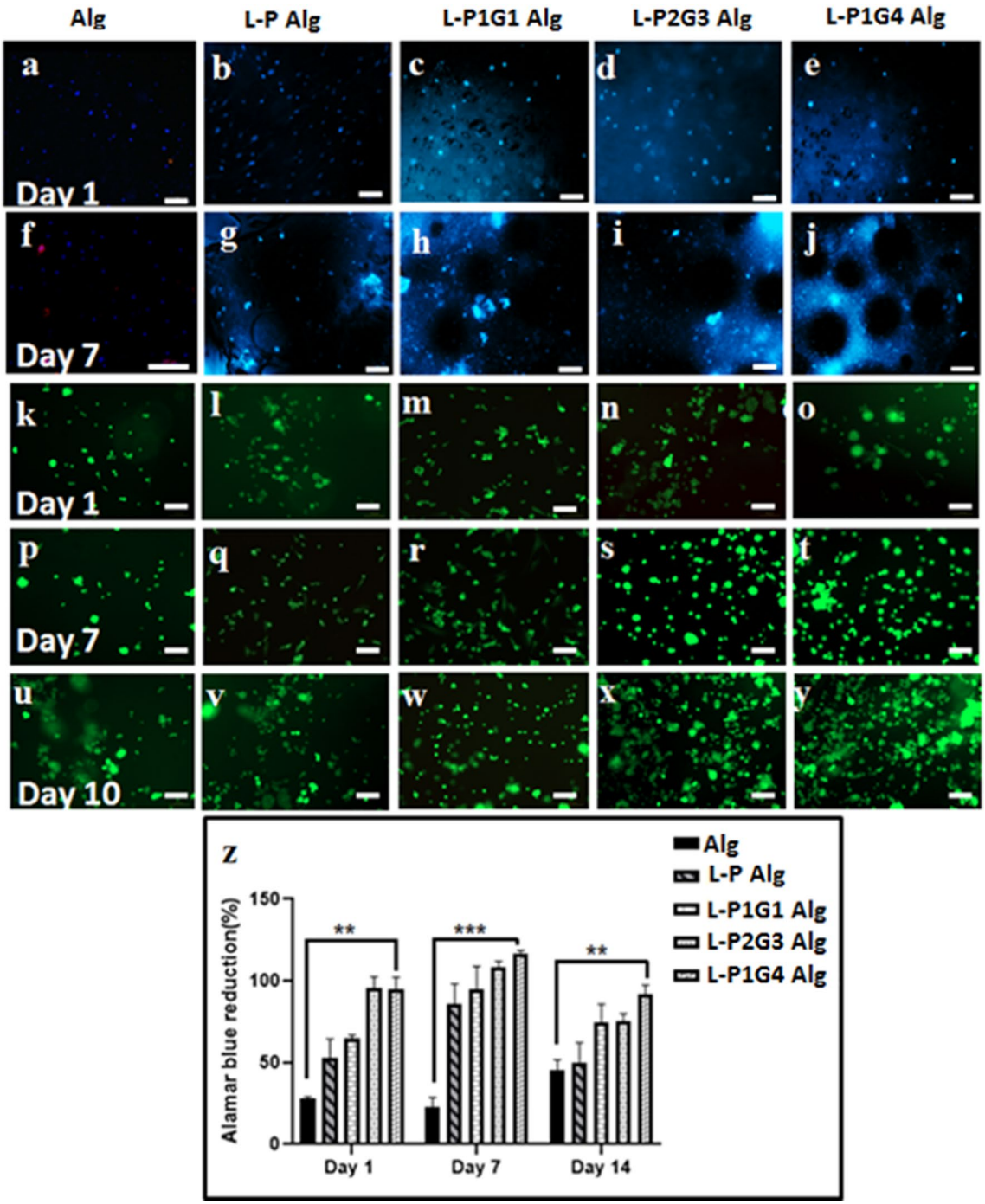

Fig. 7 Fluorescence microscopy images of hUCMSCs encapsulated within the Alg hydrogel with microbeads (**a**–**j**) encapsulated with hUCMSCs, on day 1 and day 7 (DAPI stained nuclei). Live/dead assay data of hUCMSCs encapsulated in the hydrogel with L-P, L-P1G1, L-P2G3, and L-P1G4 microbeads on day 1, day 7 and day 10 (**k**–**y**). Alamar Blue assay data of hUCMSCs encapsulated in the P and PG microbeads containing hydrogel on day 1, day 7 and day 14 (**z**). (*$P < 0.05$, **$P < 0.01$, ***$P < 0.001$) .The scale bar is 100 µm

assay (Fig. 7z). However, the cellular proliferation rate (up to 14 days of culture) in different hydrogel systems depends on the microbeads/microbead type/gelatin content of the microbeads, Fig. 7z. Thus, L-P, L-P1G1, L-P2G3, and L-P1G4 microbead hydrogels show 50%, 65%, 90%, and 97% of cell proliferation respectively, compared to only 25% for alginate hydrogel without microbeads at day 1. The proliferation of cells in different microbeads-hydrogels further increased on day 7 followed by a slight decrease in the proliferation on day 14 indicating the possible differentiation of the stem

cells (Boland et al. 2004). Significant higher proliferation in the L-P2G3 and L-P1G4 microbeads hydrogels may be associated with microbeads-mediated microenvironment modulation such as porosities within the hydrogels matrix which helps in cellular metabolite exchange, migration, and proliferation (Antoni et al. 2015).

The porosity associated with L-P2G3 and L-P1G4 hydrogels provide space for three-dimensional cellular migration when cultured for a longer duration resulting in higher cell proliferation (Tsang et al. 2007) as shown in Fig. 7z. Moreover, dissolving gelatin molecules from the microbeads (L-P1G1, L-P2G3, and L-P1G4) may intercalate into the alginate matrix and provide sites for cell adhesion and growth, which have possibly led to enhanced cellular migration and proliferation (Hiwatashi et al. 2015). It has been reported that cells embedded in modified agarose–gelatin hollow microcapsules showed enhanced proliferation and aggregation than those in unmodified agarose gel (Sakai et al. 2008), which was attributed to the combined effect of adhesiveness arising from the agarose and gelatin microcapsule membrane. Moreover, Schagemenn et al. reported chondrocytes proliferation and differentiation into the spheroidal phenotype in alginate and gelatin composite hydrogel beads (Schagemann et al. 2006).

In vitro osteoinductive capability

Osteoinductive capability of hUCMSCs was evaluated in the alginate hydrogels loaded with laponite microbeads (L-P, L-P1G1, L-P2G32, and L-P1G4). Cells were cultured for 21 days in a normal growth medium and the amount of Alkaline phosphatase (ALP) was measured to probe the osteogenic differentiation. Figure 8 shows the ALP staining of the hydrogel matrix and the quantity of ALP in different hydrogels during their culture for 21 days. L-PG microbead (P1G1, P2G3 and P1G4) hydrogels show higher alkaline phosphatase staining (Fig. 8c–e) compared to hydrogel with pectin microbeads (Fig. 8b, g) and without microbeads (Fig. 8a, f). Moreover, highly degradable L-P2G3, L-P1G4 microbeads hydrogels resulted in higher staining (Fig. 8d, e, i, j). This may be due to a large amount of leached out osteoinductive ions from laponite nanoparticles from these highly degradable sacrificial microbeads, thereby inducing osteogenic differentiation (Cui et al. 2020). The ALP staining in the L-P2G3 and L-P1G4 microbead hydrogel found to be maximum on day 14 followed by decreased activity on day 21 (Fig. 8n, o). Important to note that hydrogel with pectin (L-P) microbeads and without microbeads show minimal ALP staining (Fig. 8a, b, f, g). This is expected as ALP, being an early osteogenic differentiation marker protein, initially increases as osteoinductivity starts, followed by a decrease in activity as mineralization of the ECM proceeds, hence decreased ALP staining was observed by day 21 in L-P1G1, L-P2G3, and L-P1G4microbeadshydrogel samples (Fig. 8m–o) (Birmingham et al. 2012). The above ALP staining results were further supported by quantitative ALP assay data (Fig. 8p). Hydrogels loaded with L-P2G3 microbeads show ALP activity of 60 IU L^{-1} on day 7, followed by peak activity of 85 IU L^{-1} by day 14 as shown in Fig. 8p, whereas other microbeads (L-P, L-P1G1, and L-P1G4) loaded hydrogels show their peak of ALP activity by day 7, followed by a decrease in ALP activity. However, among different hydrogels, L-P1G4 loaded hydrogels result in the highest ALP level (70 IU L^{-1}) on day 7 but L-P2G3-loaded hydrogel shows maximum ALP activity on day 14. The fluoride doped laponite nanosilicate released from the microbeads into the alginate hydrogel matrix may have acted as an osteoinductive factor for the encapsulated stem cells, which depends on the degradation properties of the microbeads (ICP data of leached out Si-ions in the media increase from microbeads L-P to L-P1G4 shown in Figure S5 (Supplementary data).

The microbead-mediated microenvironment such as porosity, degradation, mechanical properties, and chemical cues (osteoinductive ions) played a major role in the cell attachment, migration, proliferation, and differentiation of hUCMSCs in the common alginate hydrogels matrix. Note that the alginate matrix and the amount of nanosilicate are the same in all the five different hydrogel systems evaluated in this study. The ALP activity of alginate hydrogel is 5 times lower than L-P1G4 hydrogels. Thus, superior osteogenic differentiation of stem cells in the L-PG hydrogel matrix is attributed to the difference in their 3D microenvironment which is modulated by the microbeads used here compared to hydrogel without microbeads in alginate hydrogel. It is important to note that these microbeads have their specific microenvironment of physical and chemical cues spreading within the micrometer area (size of the microbeads). Moreover, these microbeads can also modulate the microenvironment of the hydrogel matrix making it favorable for stem cell proliferation, migration and differentiation in the hydrogel matrix. One can use these microbeads and the specified hydrogel matrix for multicellular tissue regeneration by encapsulating single stem cells or two different stem/progenitor cells within the microbeads and hydrogel matrix, where two distinct microenvironments lead to specific cellular fate.

Conclusion

In the present study, we have developed a microenvironment modulating microbead-mediated porous hydrogel system consisting of two or more tailored microenvironmental niches i.e., within microbeads and hydrogel matrix. These microenvironments can be further tailored to specific encapsulated cells (stem/progenitor) for multicellular tissue

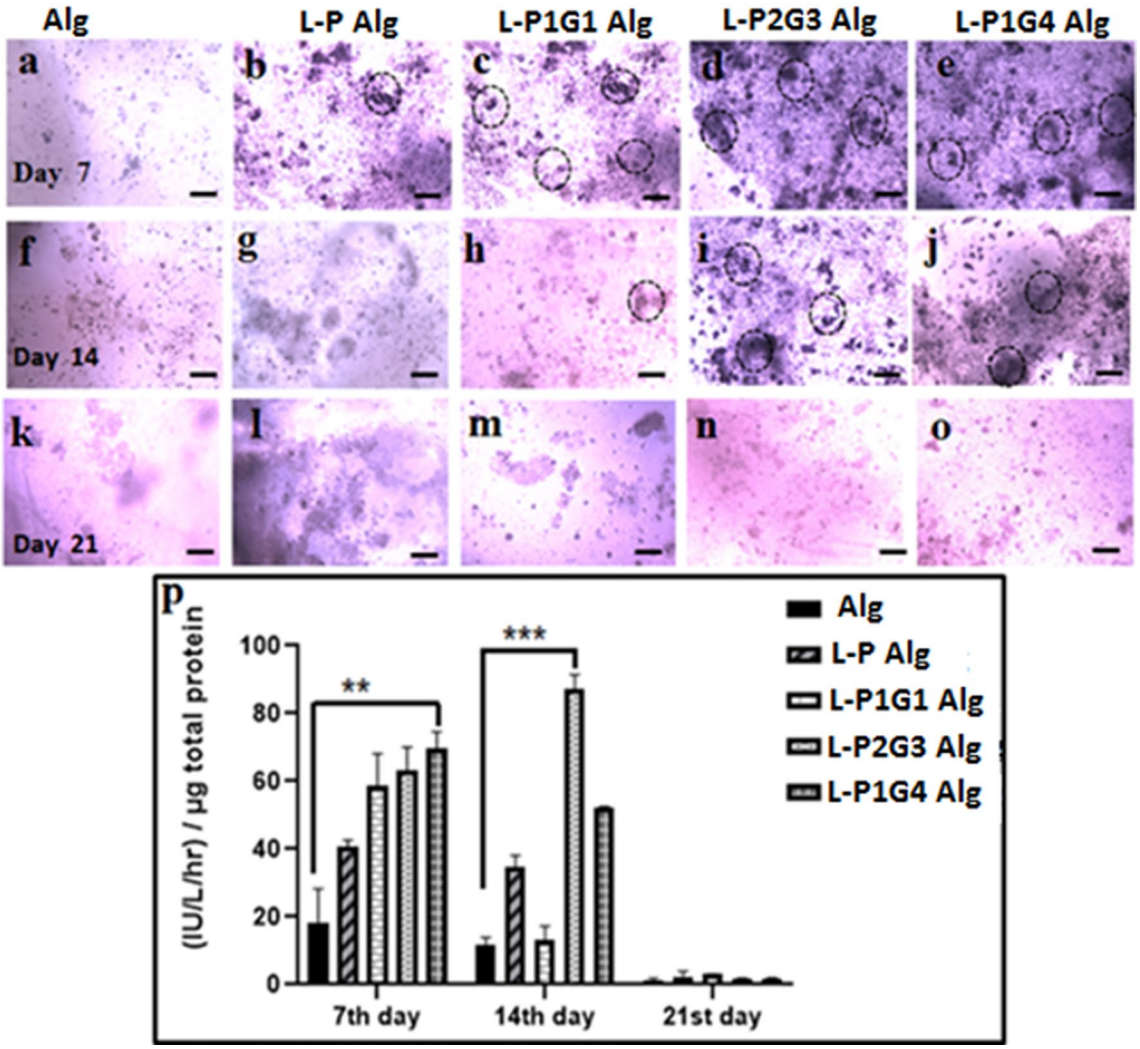

Fig. 8 Optical microscopy images of alkaline phosphatase staining of hUCMSCs encapsulated Alg (**a**, **f**, **k**), L-P Alg (**b**, **g**, **l**), L-P1G1Alg (**c**, **h**, **m**), L-P2G3Alg (**d**, **i**, **n**), L-P1G4Alg (**e**, **j**, **o**) hydrogels on day 7, day 14 and day 21. ALP activity (p) on day 7, day 14, and day 21. Scale bar is 100 µm. (*$P < 0.05$, **$P < 0.01$, ***$P < 0.001$)

regeneration. The electrospraying method of blended (pectin and gelatin) microbead preparation provides a unique platform to encapsulate cells in a sterile environment. The percent of pectin-gelatin blending along with other parameters results in microbeads with tailored size, matrix mechanics, degradability, release profiles of chemical cues, and microstructure. These microbeads can modulate the biophysical/biochemical properties of the model alginate hydrogel matrix such as stiffness, pore size, and swelling ratios depending on the pectin-gelatin ratio. We have characterized different tunable microenvironment parameters of microbeads and microbeads-loaded alginate hydrogel separately and examined their effects on stem cell (hUCMSCs) survival and proliferation. Finally, osteogenic nanosilicate-microbeads have been used to study the effect of the microenvironmental parameters of microbeads on the proliferation and osteogenic differentiation of stem cells within the hydrogel matrix (microenvironment). The microbeads-mediated hydrogel system shows enhanced stem cell function and osteogenic differentiation capability for bone tissue regeneration (as a model tissue regeneration). Moreover, unlike reported microbeads (fast degrading), controlled degradation of our microbeads results in the porous hydrogel with superior mechanical properties along with better stem cell proliferation and enhanced stem cell differentiation capacity. In this study, we have developed a simple method of microenvironment modulating microbeads and porous hydrogel system to provide two or more distinct microenvironments within the porous hydrogel and validated superior functionality of stem cells (proliferation, migration, and differentiation) in the hydrogel matrix. However, conventional hydrogel-associated microenvironment can be further modulated

using reported techniques such as functionalizing of the cell-binding ligand and growth factors, etc. This paper mainly focuses on the development of a unique porous hydrogel platform to create two or more distinct microenvironments within the 3D hydrogel and their physical/biological characterization. Additionally, one can encapsulate stem cells and/or progenitor cells into microbeads as well as hydrogel matrix with tailored microenvironmental cues for microenvironmental niche-specific cell function for multicellular tissue regeneration such as vascularized bone tissue which is under process.

Supplementary Information The online version contains supplementary material available at https://doi.org/10.1007/s40204-021-00158-3.

Funding This work was supported by the Department of Biotechnology, Ministry of Science and Technology, India (BT/RLF/Re-entry/21/2013), (BT/PR23662/NNT/28/1300/2017) and (BT/PR24271/TDS/121/40/2017), Department of Science and Technology, Ministry of Science and Technology, India (SR/NM/-NS-1364/2014(G)), and Department of Science and Technology, Ministry of Science and Technology, Science and Engineering Research Board (SERB-ECR/2015/00040, SB/S3/CE/048/2015).

Declarations

Conflict of interest The authors declare no conflict of interest.

Ethical approval All procedures performed in the study involving human participants were in accordance with the ethical standards of the Institutional Ethics Committee (IEC) and Institutional Committee for Stem Cell Research (ICSCR) of the Indian Institute of Technology, Hyderabad. IEC and ICSCR approved the entire experimental procedures associated with hUCMSCs, which includes extraction, isolation, culture, and experiment with hydrogels (IITH/IEC/2018/12).

Informed consent Informed consent was obtained from the donor.

References

Alonso-Mougán M, Meijide F, Jover A, Rodríguez-Núñez E, Vázquez-Tato J (2002) Rheological behaviour of an amide pectin. J Food Eng 55:123–129

Antoni D, Burckel H, Josset E, Noel G (2015) Three-dimensional cell culture: a breakthrough in vivo. Int J Mol Sci 16:5517–5527

Augello A, Kurth TB, De Bari C (2010) Mesenchymal stem cells: a perspective from in vitro cultures to in vivo migration and niches. Eur Cell Mater 20:e33

Bajpai S, Kirar N (2016) Swelling and drug release behavior of calcium alginate/poly (sodium acrylate) hydrogel beads. Design Monom Polym 19:89–98

Baksh D, Song L, Tuan RS (2004) Adult mesenchymal stem cells: characterization, differentiation, and application in cell and gene therapy. J Cell Mol Med 8:301–316

Benton JA, DeForest CA, Vivekanandan V, Anseth KS (2009) Photocrosslinking of gelatin macromers to synthesize porous hydrogels that promote valvular interstitial cell function. Tissue Eng Part A 15:3221–3230

Birmingham E, Niebur G, McHugh PE (2012) Osteogenic differentiation of mesenchymal stem cells is regulated by osteocyte and osteoblast cells in a simplified bone niche. Eur Cell Mater 23:13–27

Bajpai S, Sharma S (2004) Investigation of swelling/degradation behaviour of alginate beads crosslinked with Ca2+ and Ba2+ions Reactive and Functional Polymers 59:129–140

Boland GM, Perkins G, Hall DJ, Tuan RS (2004) Wnt 3a promotes proliferation and suppresses osteogenic differentiation of adult human mesenchymal stem cells. J Cell Biochem 93:1210–1230

Buwalda SJ, Boere KW, Dijkstra PJ, Feijen J, Vermonden T, Hennink WE (2014) Hydrogels in a historical perspective: from simple networks to smart materials. J Control Rel 190:254–273

Ching A, Liew C, Heng P, Chan L (2008) Impact of cross-linker on alginate matrix integrity and drug release. Int J Pharm 355:259–268

Choi S-W, Moon S-K, Chu J-Y, Lee H-W, Park T-J, Kim J-H (2012) Alginate hydrogel embedding poly (D, L-lactide-co-glycolide) porous scaffold disks for cartilage tissue engineering. Macromol Res 20:447–452

Costantini M et al (2015) Microfluidic foaming: a powerful tool for tailoring the morphological and permeability properties of sponge-like biopolymeric scaffolds. ACS Appl Mater Interfaces 7:23660–23671

Cui L et al (2020) Electroactive composite scaffold with locally expressed osteoinductive factor for synergistic bone repair upon electrical stimulation. Biomaterials 230:119617

Dang QF, Yan JQ, Li JJ, Cheng XJ, Liu CS, Chen XG (2011) Controlled gelation temperature, pore diameter and degradation of a highly porous chitosan-based hydrogel. Carbohydr Polym 83:171–178

Delorme B, Chateauvieux S, Charbord P (2006) The concept of mesenchymal stem cells

Dissanayaka WL, Hargreaves KM, Jin L, Samaranayake LP, Zhang C (2015) The interplay of dental pulp stem cells and endothelial cells in an injectable peptide hydrogel on angiogenesis and pulp regeneration in vivo. Tissue Eng Part A 21:550–563

Donati I, Benegas JC, Paoletti S (2006) Polyelectrolyte study of the calcium-induced chain association of pectate. Biomacromol 7:3439–3447

Duarte Campos DF, Blaeser A, Korsten A, Neuss S, Jäkel J, Vogt M, Fischer H (2015) The stiffness and structure of three-dimensional printed hydrogels direct the differentiation of mesenchymal stromal cells toward adipogenic and osteogenic lineages. Tissue Eng Part A 21:740–756

Estey T, Kang J, Schwendeman SP, Carpenter JF (2006) BSA degradation under acidic conditions: a model for protein instability during release from PLGA delivery systems. J Pharm Sci 95:1626–1639

Georget DM, Cairns P, Smith AC, Waldron KW (1999) Crystallinity of lyophilised carrot cell wall components. Int J Biol Macromol 26:325–331

Gohil RM (2011) Synergistic blends of natural polymers, pectin and sodium alginate. J Appl Polym Sci 120:2324–2336

Grainger SJ, Carrion B, Ceccarelli J, Putnam AJ (2013) Stromal cell identity influences the in vivo functionality of engineered capillary networks formed by co-delivery of endothelial cells and stromal cells. Tissue Eng Part A 19:1209–1222

Gryshkov O, Pogozhykh D, Hofmann N, Pogozhykh O, Mueller T (2014) Encapsulating non-human primate multipotent stromal cells in alginate

Günter EA, Popeyko OV, Belozerov VS, Martinson EA, Litvinets SG (2020) Physicochemical and swelling properties of composite gel microparticles based on alginate and callus cultures pectins with low and high degrees of methylesterification. Int J Biol Macromol 164:863–870

Gupta P, Vermani K, Garg S (2002) Hydrogels: from controlled release to pH-responsive drug delivery. Drug Discov Today 7:569–579

Guvendiren M, Burdick JA (2013) Engineering synthetic hydrogel microenvironments to instruct stem cells. Curr Opin Biotechnol 24:841–846

Haugh MG, Vaughan TJ, Madl CM, Raftery RM, McNamara LM, O'Brien FJ, Heilshorn SC (2018) Investigating the interplay between substrate stiffness and ligand chemistry in directing mesenchymal stem cell differentiation within 3D macro-porous substrates. Biomaterials 171:23–33

Hiwatashi N et al (2015) Biocompatibility and efficacy of collagen/gelatin sponge scaffold with sustained release of basic fibroblast growth factor on vocal fold fibroblasts in 3-dimensional culture. Ann Otol Rhinol Laryngol 124:116–125

Hwang CM, Sant S, Masaeli M, Kachouie NN, Zamanian B, Lee S-H, Khademhosseini A (2010) Fabrication of three-dimensional porous cell-laden hydrogel for tissue engineering. Biofabrication 2:035003

Janson IA, Putnam AJ (2015) Extracellular matrix elasticity and topography: material-based cues that affect cell function via conserved mechanisms. J Biomed Mater Res Part A 103:1246–1258

Jeon O, Bouhadir KH, Mansour JM, Alsberg E (2009) Photocrosslinked alginate hydrogels with tunable biodegradation rates and mechanical properties. Biomaterials 30:2724–2734

Keung AJ, Kumar S, Schaffer DV (2010) Presentation counts: microenvironmental regulation of stem cells by biophysical and material cues. Annu Rev Cell Dev Biol 26:533–556

Keung AJ, Kumar S, Schaffer DV (2011) Microenvironmental regulation of stem cells by biophysical and material cues. ChemInform 42

Khetan S, Guvendiren M, Legant WR, Cohen DM, Chen CS, Burdick JA (2013) Degradation-mediated cellular traction directs stem cell fate in covalently crosslinked three-dimensional hydrogels. Nat Mater 12:458–465

Kikuchi A, Kawabuchi M, Watanabe A, Sugihara M, Sakurai Y, Okano T (1999) Effect of Ca^{2+}-alginate gel dissolution on release of dextran with different molecular weights. J Control Rel 58:21–28

Kolf CM, Cho E, Tuan RS (2007) Mesenchymal stromal cells: biology of adult mesenchymal stem cells: regulation of niche, self-renewal and differentiation. Arthritis Res Ther 9:204

Lee KY, Mooney DJ (2012) Alginate: properties and biomedical applications. Progress Polym Sci 37:106–126

Lee M, Wu BM, Dunn JC (2008) Effect of scaffold architecture and pore size on smooth muscle cell growth . J Biomed Mater Res Part A 87:1010–1016

Li Y, Kilian KA (2015) Bridging the gap: from 2D cell culture to 3D microengineered extracellular matrices. Adv Healthc Mater 4:2780–2796

Lian Q, Chow Y, Esteban MA, Pei D, Tse H-F (2010) Future perspective of induced pluripotent stem cells for diagnosis, drug screening and treatment of human diseases. Thromb Haemostasis 104:39–44

Loh QL, Choong C (2013) Three-dimensional scaffolds for tissue engineering applications: role of porosity and pore size. Tissue Eng Part b Rev 19:485–502

Lutolf MP, Gilbert PM, Blau HM (2009) Designing materials to direct stem-cell fate. Nature 462:433–441

Madl CM, Heilshorn SC (2018) Engineering hydrogel microenvironments to recapitulate the stem cell niche. Annu Rev Biomed Eng 20:21–47

Mahla RS (2016) Stem cells applications in regenerative medicine and disease therapeutics. Int J Cell Biol 2016:1

Mao AS, Shin J-W, Mooney DJ (2016) Effects of substrate stiffness and cell-cell contact on mesenchymal stem cell differentiation. Biomaterials 98:184–191

Marklein RA, Burdick JA (2010) Controlling stem cell fate with material design. Adv Mater 22:175–189

Murphy CM, Haugh MG, O'brien FJ, (2010) The effect of mean pore size on cell attachment, proliferation and migration in collagen–glycosaminoglycan scaffolds for bone tissue engineering. Biomaterials 31:461–466

Muschler GF, Nakamoto C, Griffith LG (2004) Engineering principles of clinical cell-based tissue engineering. JBJS 86:1541–1558

Nichols J, Smith A (2009) Naive and primed pluripotent states. Cell Stem Cell 4:487–492

Norudin NS, Mohamed HN, Yahya NAM (2018) Controlled released alginate-inulin hydrogel: development and in-vitro characterization. In: AIP Conference Proceedings, 2018. vol 1. AIP Publishing LLC, p 020113

Park JS, Chu JS, Tsou AD, Diop R, Tang Z, Wang A, Li S (2011) The effect of matrix stiffness on the differentiation of mesenchymal stem cells in response to TGF-β. Biomaterials 32:3921–3930

Park S et al (2019) Hydrogel nanospike patch as a flexible anti-pathogenic scaffold for regulating stem cell behavior. ACS Nano 13:11181–11193

Pek YS, Wan AC, Ying JY (2010) The effect of matrix stiffness on mesenchymal stem cell differentiation in a 3D thixotropic gel. Biomaterials 31:385–391

Ramdhan T, Ching SH, Prakash S, Bhandari B (2020) Physical and mechanical properties of alginate based composite gels. Trends Food Sci Technol

Roach P, Parker T, Gadegaard N, Alexander M (2010) Surface strategies for control of neuronal cell adhesion: a review. Surf Sci Rep 65:145–173

Rosales AM, Anseth KS (2016) The design of reversible hydrogels to capture extracellular matrix dynamics. Nat Rev Mater 1:1–15

Sakai S, Hashimoto I, Kawakami K (2008) Agarose–gelatin conjugate membrane enhances proliferation of adherent cells enclosed in hollow-core microcapsules. J Biomater Sci Polym Ed 19:937–944

Sakai S, Hirose K, Taguchi K, Ogushi Y, Kawakami K (2009) An injectable, in situ enzymatically gellable, gelatin derivative for drug delivery and tissue engineering. Biomaterials 30:3371–3377

Sánchez EM et al. (2020) Hydrogels for bioprinting: a systematic review of hydrogels synthesis, bioprinting parameters, and bioprinted structures behavior. Front Bioeng Biotechnol 8

Santoro M, Tatara AM, Mikos AG (2014) Gelatin carriers for drug and cell delivery in tissue engineering. J Control Rel 190:210–218

Santos E, Hernández RM, Pedraz JL, Orive G (2012) Novel advances in the design of three-dimensional bio-scaffolds to control cell fate: translation from 2D to 3D. Trends Biotechnol 30:331–341

Schagemann JC, Mrosek EH, Landers R, Kurz H, Erggelet C (2006) Morphology and function of ovine articular cartilage chondrocytes in 3-d hydrogel culture. Cells Tissues Organs 182:89–97

Seebach C, Henrich D, Kähling C, Wilhelm K, Tami AE, Alini M, Marzi I (2010) Endothelial progenitor cells and mesenchymal stem cells seeded onto β-TCP granules enhance early vascularization and bone healing in a critical-sized bone defect in rats. Tissue Eng Part A 16:1961–1970

Shapiro L, Cohen S (1997) Novel alginate sponges for cell culture and transplantation. Biomaterials 18:583–590

Shetty P, Cooper K, Viswanathan C (2010) Comparison of proliferative and multilineage differentiation potentials of cord matrix, cord blood, and bone marrow mesenchymal stem cells. Asian J Transf Sci 4:14

Sokic S, Christenson M, Larson J, Papavasiliou G (2014) Situ generation of cell-laden porous MMP-sensitive PEGDA hydrogels by gelatin leaching. Macromol Biosci 14:731–739

Sun J, Tan H (2013) Alginate-based biomaterials for regenerative medicine applications. Materials 6:1285–1309

Thompson C, Chase GG, Yarin A, Reneker D (2007) Effects of parameters on nanofiber diameter determined from electrospinning model. Polymer 48:6913–6922

Toft K, Grasdalen H, Smidsrød O (1986) Synergistic gelation of alginates and pectins. American Chemical Society, Washington, DC

Tsang VL et al (2007) Fabrication of 3D hepatic tissues by additive photopatterning of cellular hydrogels. FASEB J 21:790–801
van den Bosch E, Gielens C (2003) Gelatin degradation at elevated temperature. Int J Biol Macromol 32:129–138
Vaziri AS, Alemzadeh I, Vossoughi M, Khorasani AC (2018) Co-microencapsulation of lactobacillus plantarum and DHA fatty acid in alginate-pectin-gelatin biocomposites. Carbohydr Polym 199:266–275
Veernala I, Giri J, Pradhan A, Polley P, Singh R, Yadava SK (2019) Effect of fluoride doping in laponite nanoplatelets on osteogenic differentiation of human dental follicle stem cells (hDFSCs). Sci Rep 9:1–15
Wagers AJ (2012) The stem cell niche in regenerative medicine. Cell Stem Cell 10:362–369
Walkenström P, Kidman S, Hermansson A-M, Rasmussen PB, Hoegh L (2003) Microstructure and rheological behaviour of alginate/pectin mixed gels. Food Hydrocolloids 17:593–603
Wang YK, Chen CS (2013) Cell adhesion and mechanical stimulation in the regulation of mesenchymal stem cell differentiation. J Cell Mol Med 17:823–832
Wang C-H, Wang T-M, Young T-H, Lai Y-K, Yen M-L (2013) The critical role of ECM proteins within the human MSC niche in endothelial differentiation. Biomaterials 34:4223–4234
Wang Y, Lee J-H, Shirahama H, Seo J, Glenn JS, Cho N-J (2016) Extracellular matrix functionalization and Huh-7.5 cell coculture promote the hepatic differentiation of human adipose-derived mesenchymal stem cells in a 3D ICC hydrogel scaffold. ACS Biomater Sci Eng 2:2255–2265
Wang X, Rivera-Bolanos N, Jiang B, Ameer GA (2019) Advanced functional biomaterials for stem cell delivery in regenerative engineering and medicine. Adv Func Mater 29:1809009
Wood JA, Liliensiek SJ, Russell P, Nealey PF, Murphy CJ (2010) Biophysical cueing and vascular endothelial cell behavior. Materials 3:1620–1639
Xu Y, Peng J, Richards G, Lu S, Eglin D (2019) Optimization of electrospray fabrication of stem cell–embedded alginate–gelatin microspheres and their assembly in 3D-printed poly (ε-caprolactone) scaffold for cartilage tissue engineering. J Orthopaed Transl 18:128–141
Yan J et al (2016) Injectable alginate/hydroxyapatite gel scaffold combined with gelatin microspheres for drug delivery and bone tissue engineering. Mater Sci Eng, C 63:274–284
Yao S et al (2016) Co-effects of matrix low elasticity and aligned topography on stem cell neurogenic differentiation and rapid neurite outgrowth. Nanoscale 8:10252–10265
Young S, Wong M, Tabata Y, Mikos AG (2005) Gelatin as a delivery vehicle for the controlled release of bioactive molecules. J Control Rel 109:256–274
Zhang Y et al (2019) Polymer fiber scaffolds for bone and cartilage tissue engineering. Adv Func Mater 29:1903279
Zhao W, Li X, Liu X, Zhang N, Wen X (2014) Effects of substrate stiffness on adipogenic and osteogenic differentiation of human mesenchymal stem cells. Mater Sci Eng C 40:316–323